Published online 30 April 2018 *Nucleic Acids Research, 2018, Vol. 46, No. 11* ***5547–5560***
doi: 10.1093/nar/gky281

The KDM4A/KDM4C/NF-κB and WDR5 epigenetic cascade regulates the activation of B cells

Kuo-Hsuan Hung[1], Yong H. Woo[2], I-Ying Lin[1], Chin-Hsiu Liu[1,3], Li-Chieh Wang[4], Hsin-Yu Chen[1], Bor-Luen Chiang[4,5] and Kuo-I Lin[1,*]

[1]Genomics Research Center, Academia Sinica, Taipei 115, Taiwan, [2]Division of Biological Sciences, King Abdullah University of Science and Technology, Thuwal 23955, Saudi Arabia, [3]PhD Program in Translational Medicine, Kaohsiung Medical University and Academia Sinica, Division of Allergy, Immunology and Rheumatology, Taipei Tzu Chi Hospital, Buddhist Tzu Chi Medical Foundation, New Taipei City 231, Taiwan, [4]Department of Pediatrics, National Taiwan University Hospital, Taipei 100, Taiwan and [5]Graduate Institute of Clinical Medicine, College of Medicine, National Taiwan University, Taipei 100, Taiwan

Received October 26, 2017; Revised March 10, 2018; Editorial Decision March 30, 2018; Accepted April 04, 2018

ABSTRACT

T follicular helper (Tfh) cell-derived signals promote activation and proliferation of antigen-primed B cells. It remains unclear whether epigenetic regulation is involved in the B cell responses to Tfh cell-derived signals. Here, we demonstrate that Tfh cell-mimicking signals induce the expression of histone demethylases KDM4A and KDM4C, and the concomitant global down-regulation of their substrates, H3K9me3/me2, in B cells. Depletion of KDM4A and KDM4C potentiates B cell activation and proliferation in response to Tfh cell-derived signals. ChIP-seq and *de novo* motif analysis reveals NF-κB p65 as a binding partner of KDM4A and KDM4C. Their co-targeting to *Wdr5*, a MLL complex member promoting H3K4 methylation, up-regulates cell cycle inhibitors *Cdkn2c* and *Cdkn3*. Thus, Tfh cell-derived signals trigger KDM4A/KDM4C - WDR5 - Cdkn2c/Cdkn3 cascade *in vitro*, an epigenetic mechanism regulating proper proliferation of activated B cells. This pathway is dysregulated in B cells from systemic lupus erythematosus patients and may represent a pathological link.

INTRODUCTION

Chromatin condensation is modified by altering the charges on histone tails. By changing the balance of charges surrounding a gene, it may activate or repress transcription. This process depends on the type, extent, and location of histone modifications. Histone methylation occurs on lysine (K) and arginine (R) residues. Methylation at K can be either mono- (me1), di- (me2) or tri- (me3); while histone R methylation can be mono- or di-, and the latter either symmetrical or asymmetrical (1). In general, trimethylation and dimethylation of histone 3 K4 (H3K4), H3K36 and H3K79 are located in euchromatic regions that are transcriptionally active, whereas trimethylation and dimethylation of H3K9, H4K20 and H3K27 are associated with transcriptionally silenced heterochromatin (2). Methylation of H3K9 is catalyzed by SET-domain containing histone lysine methyltransferases (HMTs) (3), and methyl groups are removed by histone lysine demethylases (KDMs) (4). The KDM1 family and Jumonji C (JmjC) domain-containing KDMs are the two major families of KDMs (5,6). JmjC domain-containing KDMs can be further classified into different groups based on their sequence homology and demethylase activities (7). Several KDMs are essential for development, and their dysregulation is associated with human diseases including cancer (8). For example, KDM4A and KDM4C regulate the transition of mouse embryonic stem cells to endothelial lineage (9), although KDM4A and KDM4C may appear to be dispensable in mouse embryonic development (10,11). Continual removal of H3K9 promoter methylation by KDM4 demethylases is vital for ESC self-renewal and early development (11). In spite of cumulative evidence, whether KDMs are involved in immune cell development and differentiation, such as B cell activation and differentiation, remains unclear.

Engagement of the B cell receptor (BCR) with an antigen triggers B cell activation and proliferation, thereafter inducing the differentiation of antigen-specific antibody-secreting plasma cells (12). Specialized T follicular helper (Tfh) cells located in the germinal centers (GCs) of secondary lymphoid organs promote the activation, proliferation and differentiation of B cells by providing IL-21 and CD40 ligand (13,14). Whether and how epigenetic programming is involved in the regulation of Tfh signals-mediated B cell activation is largely unknown.

*To whom correspondence should be addressed. Tel: +886 2 2787 1253; Fax: +886 2 2789 9931; Email: kuoilin@gate.sinica.edu.tw

We here found that following activation with Tfh cell-mimicking signals, B cells experience a KDM4A/KDM4C-mediated global down-regulation of H3K9me2/me3 *in vitro*. Further mapping of KDM4A/KDM4C targets using chromatin immunoprecipitation (ChIP) assays with sequencing (ChIP-seq) revealed that the WD40-repeat protein, WDR5, is important for decelerating the proliferation of activated B cells. Uncontrolled B cell activation coupled with abnormal cell cycle regulation has been linked with the pathogenesis of B cells in autoimmune diseases (15). We also demonstrate that the KDM4A/KDM4C-mediated epigenetic change, induced by Tfh-derived signals, is perturbed in activated B cells isolated from systemic lupus erythematosus (SLE) patients.

MATERIALS AND METHODS

Mice and cell cultures

MD4 transgenic mice expressing the B cell receptor with specificity for HEL in a C57BL/6 background and *Prdm1*$^{EYFP/+}$ reporter mice were purchased from The Jackson Laboratory and maintained under specific pathogen free conditions in the animal facility of the Institute of Cellular and Organismic Biology at Academia Sinica. Mouse splenic B220$^+$ B cells from mouse splenocytes were isolated by magnetic sorting with CD45R (B220) microbeads (Miltenyi Biotec) as previously described (16). The purified B220$^+$ B cells were stimulated with anti-mouse CD40 (1 μg/ml, BD Pharmingen), IL-21 (100 ng/ml, eBioscience), and HEL (1 μg/ml, Sigma-Aldrich) or LPS (2.5 μg/ml, Sigma-Aldrich). *Prdm1*$^{EYFP/+}$ reporter mice were immunized i.p. with 100 μg (4-hydroxy-3-nitrophenyl) acetyl $(NP)_{25}$-keyhole limpet hemocyanin (KLH) (Biosearch Technologies) in the primary and secondary immunizations (6 weeks apart). All animal experiments were approved by the Institutional Animal Care and Utilization Committee of Academia Sinica. Venous blood samples from SLE patients and normal healthy donors were acquired from the National Taiwan University Hospital, the Taipei Tzu Chi Hospital and the Taipei Blood Center. Patient consent procedures were approved by the National Taiwan University Hospital, Taipei Tzu Chi Hospital and Academia Sinica Research Ethics Committee. Peripheral blood B cells from SLE patients or healthy donors were purified as previously descried (16). Purified human CD19$^+$ B cells were stimulated with 10 ng/ml anti-human CD40 (R&D Systems), 200 ng/ml IL-21 (R&D Systems), 50 ng/ml BAFF (PeproTech) and 5 μg/ml anti-human IgM (Jackson ImmunoResearch). Where required, B cells were treated with 200 μM 8-hydroxyquinoline (8-HQ; EMD Millipore) or with 15 μM NF-κB inhibitor (Bay 11-7082, Calbiochem).

Lentiviral transduction and siRNA transfection

The preparation of lentiviral vectors was described previously (16). cDNA encoding WDR5 was cloned into a lentiviral vector, pFUGW (17). The detailed cloning procedures will be available upon request. B220$^+$ cells were transduced with concentrated lentiviral vectors at M.O.I. = 10 in the presence of polybrene (5 μg/ml, Sigma). The small interfering RNA (siRNA) sets for knocking down the expression of specific genes were purchased from Integrated DNA technologies. The target sense sequences of mouse FAM-tagged KDM4A siRNA are: 5′- UCUAUACAGCAUCAACUAUCUGCAC-3′ and 5′-GGCAAUUCUAGAAGCAAGGUUUGTC-3′; of mouse FAM tagged-KDM4C siRNA are 5′ GGUAGCGAGUGAUGAAGAAUUGCCT-3′ and 5′-GGAUACAAGUGGAUCAAAGCUUACT-3′. FAM-tagged WDR5 siRNA sequences are: 5′-AUAAUAAGAAUCCAAAGGUAUUGGA-3′, 5′-ACCGUGAUGGAUCAUUGAUUGUUTC-3′, and 5′-CAAGUUCAUCUGCUGAUAAACUCAT-3′.

Flow cytometric analysis

Cell surface molecules were stained by resuspending 5 × 10^5 B cells in 50 μl FACS staining buffer containing 0.1% NaN_3, 1% FCS in 1 × PBS and various fluorochrome-conjugated antigen-specific antibodies at 4°C for 15 min, followed by washing with 0.5 ml FACS staining buffer twice. 5-bromo-2′-deoxyuridine (BrdU) incorporation assay with APC-conjugated anti-BrdU (clone 3D4, 1mM, BD Pharmingen) was performed according to the manufacturer's suggestions. PKH26 cell proliferation assay is preformed according to the user's instructions of PKH26 Red Fluorescent Cell Linker Kits (Sigma-Aldrich). Final concentration of PKH26 at 2 μM was used for staining. Antibodies, all purchased from BD Pharmingen, in this study are: APC-conjugated anti-mouse CD69 (clone H1.2F3), APC-conjugated anti-mouse CD86 (clone GL1), APC-conjugated mouse B220 (clone RA3-6B2), PE-conjugated anti-mouse CD138 (clone 281-2), APC-conjugated anti-human CD69 (clone FN50), APC-conjugated anti-human CD86 (clone IT2.2), PE-conjugated anti-human IgD (clone IA6-2) and APC-conjugated anti-human CD38 (clone HB7). The fluorescence intensity was detected with FACSCanto (Becton Dickinson) flow cytometry and analyzed by the FlowJo software.

RNA isolation and RT-qPCR analysis

Total RNA was prepared from stimulated mouse splenic B220$^+$ B cells or human peripheral CD19$^+$ B cells with RNeasy Mini Kit (Qiagen). The cDNA was further synthesized by High-Capacity cDNA Reverse Transcription Kits (Thermo Fisher Scientific) with random primer mix. The cDNA was quantified by qPCR by using the SYBR green method and StepOnePlus Real-Time PCR detection systems (Applied Biosystems). The primer sequences used in this study are: *Kdm3a*: 5′-CACATTTAGGTTCCCAGTCACA-3′ and 5′ GCCACGATGTTAACACAGGA-3′, *Kdm3b*: 5′-ACTGGGTCTGTCGGAAATGTGG-3′ and 5′-CCTTTGCACACTTCAGCCAGGA-3′, *Kdm3c*: 5′-AGAAGAGGAAAGGCGAGGTC-3′ and 5′-TTGGGACCTATCTCACAGCA-3′, *Kdm4a*: 5′-TGCGGCAAGTTGAGGACAGTCT-3′ and 5′-GGATTCACAGAAAGGTCCAGTGC-3′, *Kdm4b*: 5′-GGCTTTAACTGCGCTGAGTC-3′ and 5′-GTGTGGTCCAGCACTGTGAG-3′,

Kdm4c: 5′-TGTGAAGCAGCAGGTAGCGAGT-3′ and 5′-GTCTGCCAAAGGTGGATGAGAG-3′, *Kdm4d*: 5′-AAGGTGGCATCTCAGTGCAGCT-3′ and 5′-TGTGGTCCACAACTGCCTGATC-3′, *Kdm4dl*: 5′-CATGGTCACCTTTCCCTATGG-3′ and 5′-AAAATTGATGGCCTCTGCG-3′ *Kdm6b*: 5′-AGACCTCACCATCAGCCACTGT-3′ and 5′-TCTTGGGTTTCACAGACTGGGC-3′, *Cdkn1a*: 5′-TCGCTGTCTTGCACTCTGGTGT-3′ and 5′-CCAATCTGCGCTTGGAGTGATAG-3′, *Cdkn1b*: 5′-AGCAGTGTCCAGGGATGAGGAA-3′ and 5′-TTCTTGGGCGTCTGCTCCACAG-3′, *Cdkn2a*: 5′-TGTTGAGGCTAGAGAGGATCTTG-3′ and 5′-CGAATCTGCACCGTAGTTGAGC-3′, *Cdkn2b*: 5′-ATCCCAACGCCCTGAACCGCT-3′ and 5′-AGTTGGGTTCTGCTCCGTGGAG-3′, *Cdkn2c*: 5′-GTCAACGCTCAAAATGGATTTGGG-3′ and 5′-GGATTAGCACCTCTGAGGAGAAG-3′, *Cdkn3*: 5′-ACCCTGATACATTGTTACGGAGG-3′ and 5′-CTCGAAGGCTGTCTATGGCTT-3′, *Wdr5*: 5′-CTCCTTGTGTCTGCCTCTGATG-3′ and 5′-CCTGAGACGATGAGGTTGGACT-3′, *Actb*: 5′-CATTGCTGACAGGATGCAGAAGG-3′ and 5′-TGCTGGAAGGTGGACAGTGAGG-3′, *KDM4A*: 5′-TGCGGCAAGTTGAGGATGGTCT-3′ and 5′-GCTGCTTGTTCTTCCTCCTCATC-3′, *KDM4C*: 5′-CCGATGACTCTTGTGAAGCAGC-3′ and 5′-GACTTCGTCTGCCAAAGGTGGA-3′, *WDR5*: 5′-AGTGCCTCAAGACTTTGCCAGC-3′ and 5′-CGATGAGCGTCTTCAGGCACTG-3′, *CDKN1A*: 5′-AGGTGGACCTGGAGACTCTCAG-3′ and 5′-TCCTCTTGGAGAAGATCAGCCG-3′, *CDKN1B*: 5′-ATAAGGAAGCGACCTGCAACCG-3′ and 5′-TTCTTGGGCGTCTGCTCCACAG-3′, *CDKN2A*: 5′-CTCGTGCTGATGCTACTGAGGA-3′ and 5′-GGTCGGCGCAGTTGGGCTCC-3′, *CDKN2B*: 5′-ACGGAGTCAACCGTTTCGGGAG-3′ and 5′-GGTCGGGTGAGAGTGGCAGG-3′, *CDKN2C*: 5′-CGTCAATGCACAAAATGGATTTGG-3′ and 5′-GAATGACAGCGAAACCAGTTCGG-3′, *CDKN3*: 5′-ATGGAGGGACTCCTGACATAGC-3′ and 5′-TCTCCCAAGTCCTCCATAGCAG-3′, and *Suv39h1*: 5′-CTTTGCCACAAGAACCATCTGGG-3′ and 5′-GCCAAAGTTGGAGTCCATTCGG-3′, and *ACTB*: 5′-CACCATTGGCAATGAGCGGTTC-3′ and 5′-AGGTCTTTGCGGATGTCCACGT-3′.

Immunoblot analysis and immunoprecipitation

Pre-cleared nuclear extracts or total cell extracts were prepared according to a previous protocol (18). Immunoprecipitation was performed as previously descried (18), by using pre-cleared nuclear extracts. 50 μg of nuclear extracts from various samples were incubated with 2 μg of anti-KDM4A (Abcam) or anti-KDM4C antibodies (Abcam) at 4°C for overnight and then reacting with protein A/G–sepharose (Santa Cruz Biotechnology) for 3 h. Immunoblot analysis was performed essentially following previously published protocols (18). Primary antibodies, all purchased from Abcam unless otherwise indicated, are: anti-H3K9me2 (1:500), anti-H3K9me3 (1:500), anti-H3K4me1 (1:500), anti-H3K36me2 (1:500), anti-H3K36me3 (1:400), anti-H3K27me3 (1:200), anti-H3 (1:3000), anti-KDM4A (1:150), anti-KDM4C (1:150), anti-p65 (1:300, Millipore) and anti-WDR5 (1:200). Secondary antibodies are HRP-anti-rabbit IgG (Sigma-Aldrich), HRP-anti-mouse IgG (Sigma-Aldrich), Cy2-labeled anti-rabbit IgG (Jackson ImmunoResearch) and Cy3-labeled anti-mouse IgG (Jackson ImmunoResearch). The immunoreactive proteins were detected by the enhanced chemiluminescence system (Amersham Biosciences) according to the manufacturer's protocol. The chemiluminescent or fluorescent signal images were captured using the ImageQuant LAS 4000 system (GE Healthcare Life Sciences).

Chromatin immunoprecipitation assay (ChIP) and sequential chromatin ommunoprecipitation assay (re-ChIP)

10^7 stimulated mouse B220$^+$ B cells were used per immunoprecipitation. The protein-chromatin complexes were purified by immunoaffinity captured by magnetic beads (Thermo Fisher Scientific). The enriched DNA was subjected to qPCR or deep sequencing. The re-ChIP assay was performed by using 2×10^7 stimulated B220$^+$ B cells in the first ChIP. The immunoprecipitated chromatin complexes from the first ChIP assay were eluted by DTT-containing elution Buffer (10 mM DTT, 0.2% SDS in 1 × TE buffer) for 30 min at 37°C and then were further diluted 20-fold in a dilution buffer (10 mM Tris–HCl, pH8.0, 1 mM EDTA, 0.5 M EGTA, 100 mM NaCl, 1% Triton X-100 and protease inhibitor cocktail [Roche]), followed by the second ChIP. DNA in the IP was quantified by qPCR. The antibodies used in ChIP are: anti-H3K9me2, (Abcam), anti-H3K9me3 (Abcam), anti-KDM4A (Abcam), anti-KDM4C (Abcam) and anti-H3K4me3 (Abcam). The primer sequences used in ChIP qPCR are: *Wdr5*-1: 5′-GAAGCATATCAAGGATGGTAT-3′ and 5′-TCTGAGGACCATGACTTGTATG-3′, *Wdr5*-2: 5′-TACATTGTGCTTATAGACC-3′ and 5′-GTCTCAATAGCTAATTTAG-3′, *Wdr5*-3: 5′-TACTGGGAAGTAGACTTTACTG-3′ and 5′-AGCAGTTTCAGACTTGGT-3′, *Wdr5*-4: 5′-TACTTGTTAAAGACGCTGACA-3′ and 5′-TGTCGTACAATACTCTCTAAC-3′, *Wdr5*-5: 5′-CTTAGAACGACTAATGGAGGCT-3′ and 5′-GTAGCTTTCTCTTAATATCAGAG-3′, *Cdkn2a*-1: 5'-TCTGTGGAGCTAACCCAAGG-3' and 5'-TGTGACTTTGCAGTGGAACC-3', *Cdkn2a*-2: 5'-CGCTCTATAAGACCCTGCCA-3' and 5'-TGAGACTTGGTGGCCTTTCA-3', *Cdkn3*-1: 5′-AGCCAATCCCCTTTCTTCC-3′ and 5′-GCGTTCCAGAAACCAATCAT-3′, and *Cdkn3*-2: 5′-GTGGCAGATCTGTGGCACT-3′ and 5′-CTCACAAACGGGGTCGTTAC-3′.

ChIP-seq

ChIP-seq libraries were prepared using standard protocols provided by Illumina (www.illumina.com). Libraries were sequenced (Solexa, Illumina) in two successive runs and output from each sample was used for analysis. The resulting sequence outputs (bases 2-42) were aligned to the ref-

erence mouse genome (version mm9) using bowtie 0.12.7 (19).

The peaks were filtered for $P < 10^{-20}$, next, peak calling and annotation were done by using Model-based Analysis of ChIP-Seq (MACS, version 1.4) (20) and peakAnnotator (version 1.4) (21), respectively. The published ChIP-seq data from Gene Expression Omnibus (GEO) database were acquired to analyze the binding targets of H3K9me2 and H3K9me3 (accession number GSE82144) (22), RELA (GSE36099) (23), and KDM4A and KDM4C in mouse acute myeloid leukemia (AML) cells (GSE81300) (24).

Motif discovery

For *de novo* motif prediction analysis of ChIP-seq results, HOMER motif analysis software (25) was used to identify among the KDM4A/KDM4C binding regions over-represented DNA sequence motifs. From the summit of the ChIP-seq binding peak, we extended the genomic region by 500 bp on either side to obtain a 1000-bp region, to be scanned for over-represented DNA sequence motifs. The over-represented DNA motif-sequences were compared with known motifs of transcription factors.

Microarray and gene ontology (GO) analysis

Total RNA from 10^7 stimulated mouse B220$^+$ B cells was extracted with TRIzol reagent (Thermo Fisher Scientific) according to the manufacturer's instructions. Approximately 2 μg of RNA was labeled and hybridized to GeneChip Mouse Genome 430 2.0 arrays (Affymetrix) according to the manufacturer's protocols. All data analysis was performed using GeneSpring software GX 7.3.1 (Agilent Technologies). GO analysis of differentially expressed genes was performed using the Biological Networks Gene Ontology (BiNGO) program package with $P \leq 0.05$ (26). The ten most significant terms in the Biological Process ontology were selected to show the functional characteristics of the given gene sets.

Statistical analysis

Statistical analysis was performed based on a two-tailed *t* test. $P < 0.5$ was considered statistically significant.

RESULTS

Induction of KDM4A and KDM4C is associated with down-regulation of H3K9me2/me3 in B cells after exposure to Tfh cell-derived signals

We first examined the expression of various histone markers and histone modifying enzymes in mouse splenic B cells exposed to Tfh cell-derived signals. Primary splenic B cells isolated from MD4 transgenic mice that carry the BCR with specificity for hen egg lysozyme (HEL; (27)) were stimulated with IL-21, anti-CD40 and HEL, to mimic the exposure of Tfh cell-derived signals in antigen-primed B cell responses (13,14). Remarkably, immunoblotting using nuclear extracts and a panel of antibodies specific for acetylation (ac), me2 or me3 at K4, K9, K27 and K36 of H3 revealed that global H3K9me2/me3 and H3K36me2/me3 levels start to decline 24 h after stimulation (Figure 1A) and remain down-regulated at 48 h. Other histone markers did not change substantially (Figure 1A) and similar results were found when histone extracts were used instead (Supplementary Figure S1A). To determine whether the decreased histone methylation is a result of up-regulation of KDMs, we examined KDM expression in splenic B cells treated with Tfh cell-mimicking stimuli. Among those examined, mRNA levels of *Kdm4a* and *Kdm4c* which encode demethyalses specific for H3K9me2/me3 and H3K36me2/me3, were most significantly up-regulated from 18 h after stimulation (Figure 1B and Supplementary Figure S1B). Accordingly, KDM4A and KDM4C protein levels were dramatically increased (Figure 1C) and were inversely associated with the reduced H3K9me2/me3 and H3K36me2/me3 levels. However, activation of B cells by lipopolysaccharide (LPS) treatment neither substantially up-regulated KDM4A and KDM4C nor caused reduction of H3K9me2/me3 (Figure 1D). Moreover, reduced global H3K9me2/me3 and H3K36me2/me3 levels and induction of KDM4A and KDM4C were not limited to stimulation with the BCR-specific antigen, HEL; similar expression patterns were observed when anti-IgM was applied to ligate the BCR together with IL-21 and anti-CD40 treatment (Supplementary Figure S1C and D). *Kdm3b* was also up-regulated substantially in B cells responding to Tfh-mediated signals (Supplementary Figure S1B). However, because KDM3B demethylases H3K9me2/me1 (28), which is not detected by our antibody panel, we chose to focus on KDM4A and KDM4C in this study. Also, given that KDM4-dependent control of H3K9me3 levels at gene promoters is crucial for transcriptional activity (11), we hereafter focus on the effects of the connection between KDM4A/KDM4C and H3K9me2/me3 on B cell activation. Together, we show that global H3K9me3 levels are decreased in activated B cells exposed to Tfh-cell mimicking signals *in vitro*.

Depletion of KDM4A and KDM4C prolongs B cell activation and proliferation

We next sought to investigate the functional effects of KDM4A and KDM4C on B cells stimulated with Tfh-cell mimicking signals. Transfection of siRNA-pools against *Kdm4a* and *Kdm4c* into mouse splenic B cells after stimulation largely blocked the reduction of H3K9me2/me3, as compared with cells transfected with control siRNA carrying scramble sequence (siCtrl; Figure 2A). The up-regulation kinetics of surface CD69 and CD86 was prolonged in siKDM4A- or siKDM4C-transfected cells (Figure 2B and C). CD69 and CD86 levels peaked at 18 and 24 h, respectively, after stimulation of siCtrl-transfected cells. In contrast, CD69 and CD86 levels on siKDM4A- or siKDM4C-transfected cells were sustained at high levels at 48 h. In addition, the abundances of BrdU positive cells were increased in KDM4A- and KDM4C-depleted cells at 24, 36 and 48 h after stimulation, as compared those in siCtrl-transfected cells (Figure 2D). The enhanced B cell activation and proliferation may not result from the off-target effects of siRNA-pools because two individual siRNAs against *Kdm4a* and *Kdm4c* also give rise to similar results (Supplementary Figure S2). Combined, these data

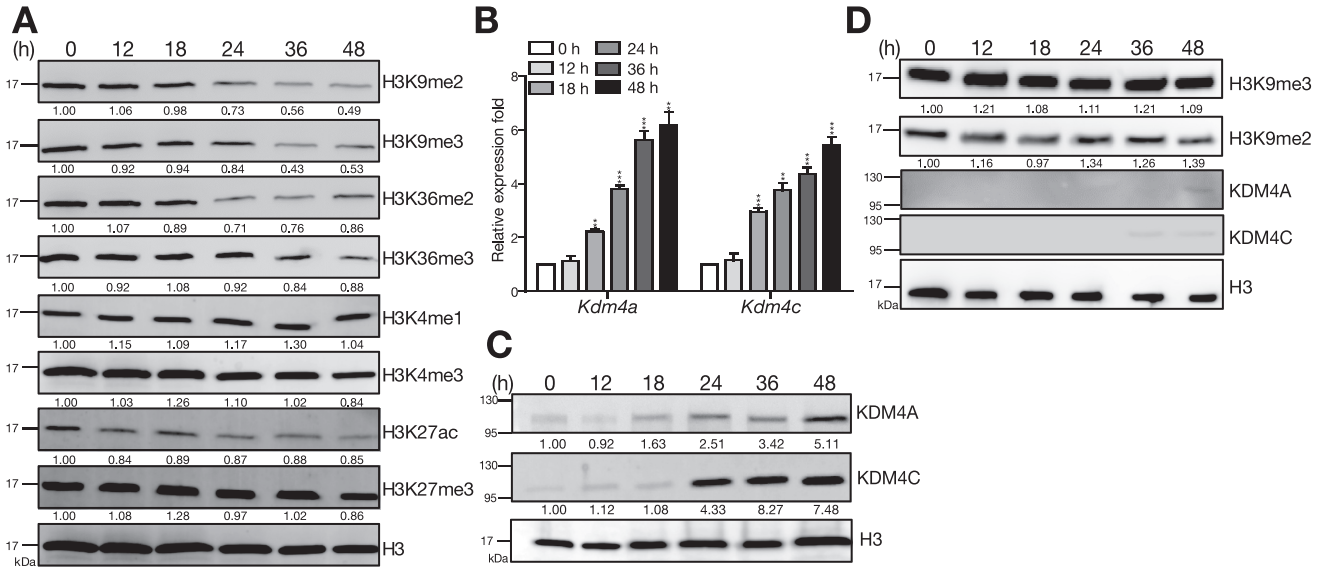

Figure 1. Up-regulation of KDM4A and KDM4C and reduction of H3K9me2/me3 is found following stimulation of B cells by Tfh-cell derived signals. (**A**) Levels of histone markers detected by immunoblotting (IB) with nuclear extracts from [HEL + anti-CD40 + IL-21]-stimulated splenic B cells from MD4 mice at indicated time points. (**B**, **C**) *Kdm4a* and *Kdm4c* mRNA (B) and protein (C) levels at indicated time points in stimulated splenic B cells isolated from MD4 mice. Lamin B was used as the protein loading control in (C). (**D**) Levels of H3K9me2, H3K9me3, KDM4A, and KDM4C detected by IB with nuclear extracts from LPS (2.5 μg/ml) stimulated splenic B cells from C57BL/6 mice at indicated time points. H3 is served as the loading control. The relative levels of indicated proteins in (A) (C) and (D) after quantification were indicated. Results in (B) represent the mean ± SEM ($n = 3$). $^{**}P < 0.01$, $^{***}P < 0.005$ (Student's *t*-test).

suggest that depletion of KDM4A or KDM4C results in prolonged B cell activation and enhanced B cell proliferation in response to signals derived from Tfh cells.

KDM4A and KDM4C associate with NF-κB in activated B cells

Given that KDM4A and KDM4C lack site-specific DNA binding capacities, we next sought to identify the transcription factors that collaborate with KDM4A or KDM4C to regulate the activation and proliferation of B cells when encountering Tfh cell-mimicking signals. Toward this end, we performed ChIP-seq to profile the genome-wide binding of KDM4A and KDM4C in splenic B cells stimulated with Tfh-mimicking signals. Analysis of the common peak sequences of KDM4A and KDM4C from ChIP-seq data with *de novo* motif discovery programs identified a KDM4A and KDM4C binding motif (Figure 3A). This motif found in the vicinity of KDM4A and KDM4C-specific peaks shares the known motifs with transcription factors TEA domain transcription factor 4 (TEAD4), TEAD3 and NF-κB p65 (RELA) (Figure 3B). However, given that TEAD4 and TEAD3 binding sites resemble to the NF-κB site (29), and that NF-κB is critical for activation and proliferation of B cells, we chose to examine the involvement of NF-κB on the effects of KDM4A and KDM4C during Tfh cell-mimicking signals-mediated B cell activation.

Nuclear extracts isolated from mouse splenic B cells treated with Tfh cell-mimicking stimuli for 0, 24 and 48 h were subjected to co-immunoprecipitation (co-IP) to examine the interaction of NF-κB p65 and KDM4A or KDM4C. KDM4A and KDM4C form a complex at 24 and 48 h after stimulation because either one of them can be immunoprecipitated by an antibody against the other (Figure 3C). Notably, NF-κB p65 can be detected in anti-KDM4A and anti-KDM4C immunoprecipitates 24 h after stimulation (Figure 3D). However, the interaction between KDM4A, KDM4C and NF-κB p65 is reduced at 48 h, despite them all being expressed in the nucleus (Figure 3C). Next, a sub-optimal dose of the NF-κB inhibitor, Bay 11-7082 was used to treat stimulated B cells, which is thought to bypass the cytotoxicity effects caused by the complete blockage of NF-κB activation. Remarkably, the global reduction of H3K9me2/me3 after B cell stimulation was largely rescued in the presence of NF-κB inhibitor as compared with those in solvent control DMSO-treated cells (Figure 3D). These results suggest that temporal association of KDM4A, KDM4C and NF-κB cooperatively establishes the global changes in H3K9me2/me3 following activation of B cells.

Genome-wide analysis identifies *Wdr5* as the KDM4A/KDM4C target in activated B cells

KDM4A and KDM4C target loci were mapped by computational analysis of ChIP-seq data. We obtained approximate 5 million uniquely aligned reads and further used model-based analysis of ChIP-seq (MACS) to identify 1187 KDM4A–bound regions and 1240 KDM4C–bound regions in activated B cells (Supplementary Table S1). Most of the KDM4A- and KDM4C–bound regions were distal and intergenic regions, but some were annotated to 246 and 264 genes (Supplementary Table S2), respectively. Interestingly, a large proportion of targets are co-occupied by both KDM4A and KDM4C; 68.3% of KDM4A peaks overlapped with 63.6% of KDM4C peaks in activated B cells (Figure 4A), supporting the hypothesis that KDM4A and

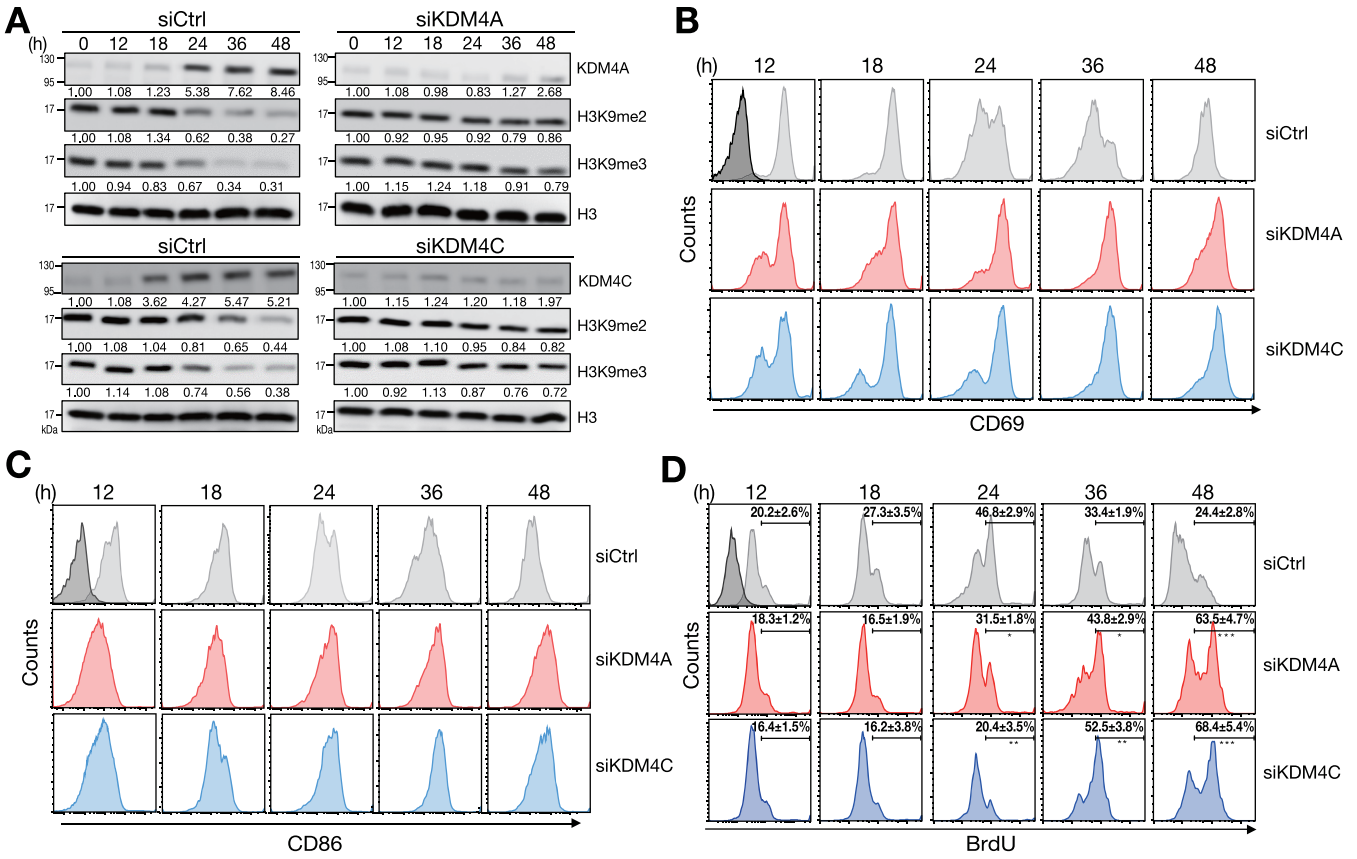

Figure 2. B cell activation and proliferation sustains by depletion of KDM4A or KDM4C. (**A**) Immunoblot showing the levels of KDM4A, KDM4C and H3K9me2/me3 histone modification markers in [HEL + anti-CD40 + IL-21]-stimulated MD4 splenic B cells transfected with control siRNA or siRNA-pools against KDM4A or KDM4C. (B, C) FACS analysis showing the levels of activation markers CD69 (**B**) and CD86 (**C**) on stimulated MD4 splenic B cells after depletion of KDM4A or KDM4C at indicated time points. (**D**) FACS analysis showing the frequencies of BrdU incorporation in stimulated MD4 splenic B cells transfected with siCtrl, siKDM4A- or siKDM4C-pools at indicated time points. Relative levels of indicated proteins in (A) after quantification were indicated. Results are the mean ± SD ($n = 3$) in (D). *$P < 0.05$, **$P < 0.01$, *** $P < 0.005$ (Student's t-test). Dark-shaded histograms in (B), (C) and (D) represent the levels of indicated molecules at day 0.

KDM4C elicit their effects as a protein complex.

Gene expression profiles in KDM4A- and KDM4C-depleted B cells stimulated with Tfh cell-mimicking signals for 0, 24 and 72 h were investigated using microarray analysis. Genes showing at least 1.5-fold up- or down-regulation in KDM4A and KDM4C knockdown cells after stimulation are listed in Supplementary Table S3. Among these genes, *Wdr5* is a core subunit of the SET1/MLL or COMPASS complexes that facilitates the assembly and activity of complexes (30), but the role of WDR5 in B cells is unknown. We observed KDM4A and KDM4C binding in broad genomic regions 5′ distal to *Wdr5* (Figure 4B). These results were further validated by an independent ChIP experiment (Figure 4C). Further combined analysis of the previously published ChIP-seq data of histone marks of activated B cells (22) showed that the distribution of H3K9me2 and H3K9me3 was predominantly located at the region upstream of *Wdr5* and their enriched peaks were decreased after stimulation (Figure 4B).

More importantly, KDM4A and KDM4C are required for the up-regulation of *Wdr5*, as knocking down the expression of KDM4A or KDM4C dramatically blocked *Wdr5* induction after stimulation as compared with siCtrl transfected B cells (Figure 4D). This effect was associated with the increased levels of H3K9me2/me3 on *Wdr5* in KDM4A or KDM4C knockdown B cells (Figure 4E). Given that KDM4A, KDM4C and NF-κB p65 form a complex, we next examined whether NF-κB p65 also participates in the regulation of *Wdr5*. Our sequential ChIP (re-ChIP) assay using either anti-p65 or control rabbit IgG (rIgG) in the first ChIP and then anti-KDM4A, anti-KDM4C, or rIgG in the re-ChIP, showed that NF-κB p65 binds, together with either KDM4A or KDM4C, to *Wdr5* gene loci 24 h after stimulation (Figure 4F). Furthermore, treatment with the NF-κB inhibitor Bay 11-7082 results in reduced *Wdr5* mRNA (Figure 4G) and increased H3K9me2/me3 levels at some *Wdr5* loci (Figure 4H) in stimulated B cells. Together, these results indicate that NF-κB, together with KDM4A and KDM4C, is needed for the transcription of *Wdr5* in B cells primed with Tfh cell-mimicking signals.

WDR5 regulates B cell proliferation and activates cyclin-dependent kinase inhibitors (CDKNs)

We next depleted WDR5 by transfecting three independent siRNAs or siRNA-pools against *Wdr5* into purified

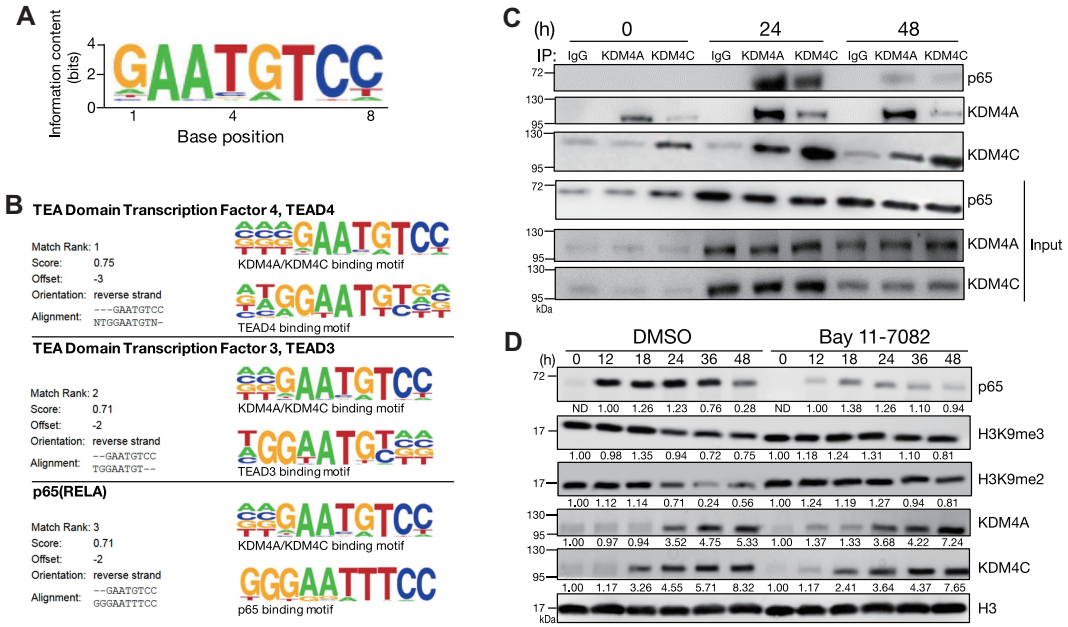

Figure 3. KDM4A, KDM4C and NF-κB temporarily form a complex during B cell activation. (**A**) Consensus KDM4A and KDM4C-binding motif identified using the *de novo* motif-discovery program Homer Software, $P = 1 \times 10^{-42}$. (**B**) Analysis of *de novo* discovery of ChIP-seq peaks derived from the common motif of KDM4A and KDM4C binding sites revealed the top three transcription factor binding motifs. (**C**) Co-immunoprecipitation (co-IP) using nuclear extracts from MD4 mouse splenic B cells stimulated with HEL + anti-CD40 + IL-21, followed by immunoblot showing the interaction of NF-κB p65 with KDM4A and KDM4C 24 h after stimulation. Rabbit IgG was used as the control antibody in the immunoprecipitation. (**D**) Immunoblot and quantitative analysis showing the levels of indicated nuclear proteins in stimulated MD4 mouse splenic B cells treated with 15 μM of BAY 11-7082 NF-κB inhibitor at indicated time points. Relative levels of indicated proteins in (D) after quantification were indicated.

B cells to determine the effect of WDR5 on B cell activation and proliferation. Depletion of WDR5 resulted in the enhanced induction of CD69 and CD86 in stimulated B cells at 48 and 72 h (Figure 5A and B and Supplementary Figure S3A-B). Furthermore, proliferation was significantly augmented in WDR5 knockdown cells treated with Tfh cell-mimicking signals (Figure 5C and Supplementary Figure S3C). These findings are similar to the effects of KDM4A and KDM4C knockdown in stimulated B cells. To determine whether WDR5 is a critical downstream target of KDM4A and KDM4C, we reintroduced WDR5 via a lentiviral vector (Figure 5D) in stimulated B cells that were also transfected with siKDM4A-pools and siKDM4C-pools. As compared with cells transfected with siCtrl group, KDM4A and KDM4C depletion and transduction with control lentiviral vector not only decreased WDR5 mRNA in mouse splenic B cells stimulated with Tfh-mimicking signals (Figure 5D) but also enhanced the induction of CD69 and CD86 activation markers (Figure 5E–G) and increased proliferation (Figure 5H). Moreover, reintroduction of WDR5 abrogated the enhanced induction of activation markers (Figure 5E–G) and proliferation (Figure 5H) in KDM4A and KDM4C depleted cells. These results suggest that WDR5 is an important target of KDM4A and KDM4C in the control of B cell activation and proliferation. However, overexpression of WDR5 alone did not significantly alter B cell activation and proliferation primed by Tfh-cell mimicking signals (Figure 5D−H).

We next dissected the mechanistic insights of the function of WDR5 in activated B cells. We re-visited the cDNA microarray data of KDM4A or KDM4C depleted B cells that were stimulated with Tfh cell-mimicking signals (Supplementary Table S3). Gene Ontology (GO) analysis of these differentially expressed genes that are affected by knockdown of KDM4A or KDM4C revealed that 'cell cycle' was among the top 10 enriched GO categories 72 h after stimulation (Supplementary Figure S4). Among the genes in this category, we noticed that the expression of several CDKNs is closely regulated by KDM4C and KDM4C (Figure 6A). CDKNs arrest the cell cycle by interfering with the interaction between cyclins and cyclin-dependent kinases (CDKs) that promote cell cycle progression (31). Using RT-qPCR array and RT-qPCR, we further showed that the expression of these CDKNs was concomitantly down-regulated in WDR5 knockdown splenic B cells (Figure 6B and C). In particular, *Cdkn2a* and *Cdkn3* levels were accordingly reduced when KDM4A or KDM4C was depleted (Figure 6C). Moreover, reduced *Cdkn2a* and *Cdkn3* expression is associated with decreased H3K4me3 levels at their gene loci in WDR5-depleted B cells (Figure 6D). H3K4me3 levels at *Cdkn2a* and *Cdkn3* loci were consistently reduced in KDM4A or KDM4C knockdown B cells, and depletion of both in stimulated B cells caused more significantly reduced H3K4me3 levels at *Cdkn2a* and *Cdkn3* loci (Figure 6E). We further found that the expression of *Cdkn2a*, *Cdkn2c* and *Cdkn*3 was reduced after inhibition of NF-κB activity by BAY-117082 treatment, and their expression was recovered after reintroduction of WDR5 (Figure 6F). To further evaluate the potential function of KDM4A/KDM4C in immune responses *in vivo*, we immunized *Prdm1*$^{EYFP/+}$ reporter mice with T cell-dependent antigen NP-keyhole limpet hemocyanin (NP-KLH). These mice carry the en-

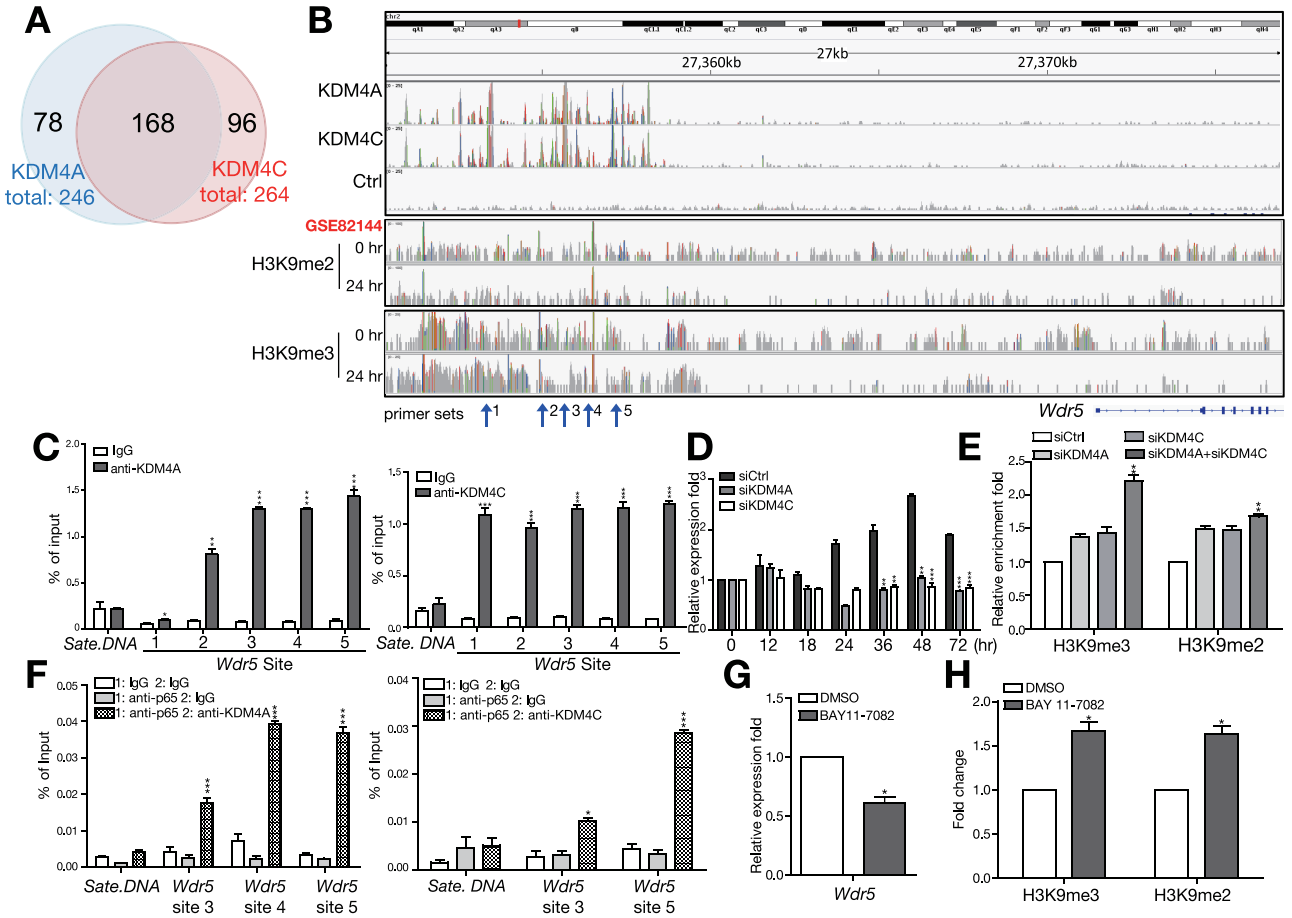

Figure 4. *WDR5* is identified as the direct target of KDM4A and KDM4C in activated B cells primed by Tfh-derived signals. (**A**) Venn diagram of the number of overlapping genes identified by ChIP-seq with anti-KDM4A and anti-KDM4C. (**B**) Representative Integrative Genomics Viewer (IGV) tracks near *Wdr5* loci showing the binding profiles of KDM4A, KDM4C and indicated histone marks. Tracks from top to bottom are ChIP-seq peaks of KDM4A, KDM4C, Ctrl in 24 hr stimulated with HEL + anti-CD40 + IL-21 in B cells, ChIP-seq peaks of H3K9me2 and H3K9me3 in resting or stimulated B cells. (**C**) qPCR using primer sets indicated in (B) and anti-KDM4A (left panel) and anti-KDM4C (right panel) immunoprecipitated chromatin from MD4 mouse splenic B cells stimulated with HEL + anti-CD40 + IL-21 for 24 h. Satellite DNA (Sate. DNA) was used as the negative control locus. (**D**) RT-qPCR showing *Wdr5* mRNA levels in stimulated MD4 B cells transfected with indicated siRNA at various time points. (**E**) ChIP showing the levels of H3K9me2/me3 on *Wdr5* site 5 in stimulated B cells transfected with indicated siRNA. (**F**) ChIP and re-ChIP showing the co-binding of NF-κB p65 with KDM4A (left panel) or KDM4C (right panel) to indicated *Wdr5* loci in stimulated MD4 B cells at 24 h. (**G**) RT-qPCR showing the levels of *WDR5* mRNA in stimulated B cells treated with DMSO or 15 μM BAY 11-7082 for 24 h. (**H**) ChIP showing the levels of H3K9me2/me3 on *WDR5* in stimulated B cells in (G). Results in (**C**)–(**H**) represent the mean ± SEM ($n = 3$). *$P < 0.05$, **$P < 0.01$, *** $P < 0.005$ (Student's t-test).

hanced yellow fluorescence protein *(EYFP)* reporter gene under the control of the endogenous plasma cell *Prdm1* gene promoter (32). B220$^+$ splenic B cells from naïve mice, EYFP$^-$B220$^+$CD95$^+$ GC B cells from *Prdm1*$^{EYFP/+}$ mice 2 weeks after primary immunization, and EYFP$^+$CD138$^+$ bone marrow plasma cells from *Prdm1*$^{EYFP/+}$ mice 1 week after secondary immunization were sorted to examine the expression of *Kdm4a*, *Kdm4c* and their downstream targets (Figure 6G). Compared with naïve B cells, mRNA levels of *Kdm4a* and *Kdm4c* as well as their target, *Wdr5* were increased in GC B cells and sustained in bone marrow plasma cells. *Cdkn2a* and *Cdkn3* expression levels are higher in bone marrow plasma cells than in GC B cells (Figure 6H). Taken together, our data revealed that NF-κB participated KDM4A/KDM4C and WDR5 epigenetic cascades program the initiation of cell cycle arrest genes following exposure to Tfh cell-derived signals.

Abnormal expression of KDM4A and KDM4C is found in SLE B cells

In parallel, we investigated whether up-regulation of *KDM4A* and *KDM4C* also occurred in human B cells responding to Tfh cell-mimicking signals. Moreover, we sought to examine whether their expression is dysregulated in B cells isolated from human SLE patients, which exhibit hyperreactivity. We compared the expression of *KDM4A* and *KDM4C* in peripheral blood B cells isolated from healthy donors and SLE patients and subsequently stimulated with IL-21, anti-CD40, B-cell activating factor (BAFF), and anti-IgM. Compared with normal human B cells, SLE B cells indeed showed enhanced B cell activation, as characterized by elevated induction of CD69 and augmented proliferation after stimulation (Supplementary Figure S5A and B). The mRNA levels of *KDM4A* and *KDM4C* induced in normal human B cells following stim-

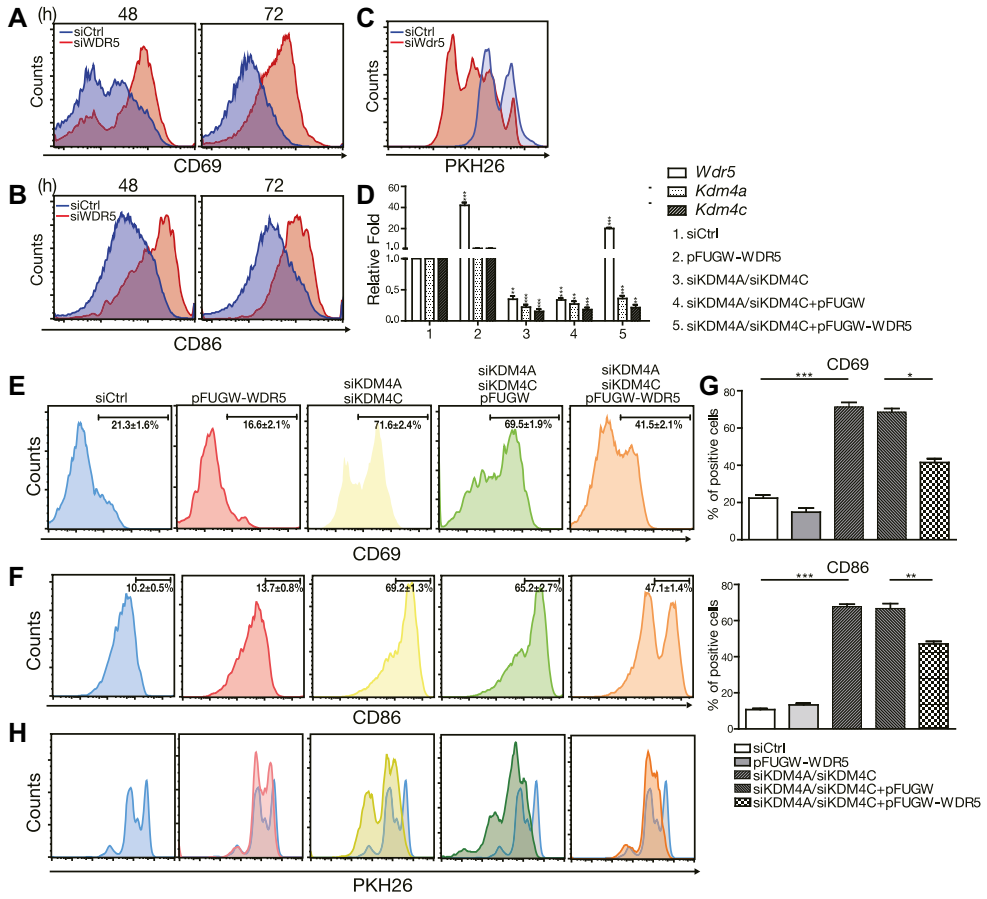

Figure 5. WDR5 regulates B cell activation. (A, B) FACS analysis showing the levels of surface CD69 (**A**) and CD86 (**B**) on [HEL + anti-CD40 + IL-21]-stimulated MD4 mouse splenic B cells depleted of WDR5 by siRNA-pools. (**C**) PKH26 labeling assay showing cell proliferation of siCtrl or siWdr5-pools transfected MD4 B cells, and [HEL + anti-CD40 + IL-21]-stimulated MD4 B cells. (**D**) The indicated mRNA levels from 3-day [HEL + anti-CD40 + IL-21]-stimulated MD4 B cells treated with the indicated reagents, siCtrl or siWDR5-pools, and/or lentiviral vector alone (vector) or vector expressing WDR5. (E–H) FACS analysis of cells from (D) showing the levels of surface CD69 (**E**) and CD86 (**F**) as well as the dilution of PKH26 (H). Bar graphs of the percentage of CD69 (E) and CD86 (F) positive cells were shown in (**G**). Blue histograms in (H) are overlaid from the DMSO treated group for comparison. Results in (D)-(G) represent the mean ± SEM ($n = 3$). *$P < 0.05$, ** $P < 0.01$, *** $P < 0.005$ (Student's t-test).

ulation (Figure 7A and B) were consistent with their up-regulation in mouse B cells primed with Tfh cell-mimicking signals. It is noted that *KDM4A* and *KDM4C* levels were significantly reduced in the steady state, as well as in the stimulated SLE B cells, as compared with normal B cells (Figure 7A and B). We then sought to determine whether the epigenetic changes could be observed in SLE B cells. It is noted that, the activated normal human B cells exhibited a broad reduction of H3K9me2 and H3K9me3 (Figure 7C). By contrast, the levels of H3K9me2 and H3K9me3 in stimulated SLE B cells did not appear to significantly change (Figure 7C). The expression of *WDR5* mRNA as well as several *CDKNs*, including *CDKN2A* and *CDKN3*, in stimulated B cells, was reduced in stimulated SLE B cells as compared with that in stimulated normal B cells (Figure 7D and E). Further, treatment with a KDM4 inhibitor, 5-carboxy-8-HQ (8-HQ; (33)) in stimulated normal human peripheral B cells not only resulted in enhanced and prolonged activation of CD69 and CD86 (Supplementary Figure S5C and D) but also reduced *WDR5* mRNA (Figure 7F) and enhanced proliferation (Figure 7G), as compared with DMSO solvent control treated and stimulated normal peripheral B cells. Combined, these results suggest that aberrant expression of KDM4A, KDM4C and WDR5 in SLE B cells treated with Tfh-cell mimicking signals may be associated with their enhanced activation and proliferation in this disease.

DISCUSSION

Although it has been reported that the global levels of H3K9me2/me3 and H3K4me2 are all up-regulated at 72 h after LPS and IL-4 stimulation in B cells (34), the overall changes in histone modification in response to Tfh cell-mimicking signals in B cells are still unclear. In this study, we show the global reduction of H3K9me2/me3 in B cells responding to Tfh cell-mimicking signals, but not LPS stimulation. Methylation of H3K9 has been implicated in heterochromatin formation and gene silencing. Trimethylation on H3K9 is added by HMTs such as SUV39H1, and removed by the KDM4 family (35). Different HMTs have distinct target loci; for example, SUV39h1 in mouse cells is enriched in major satellite pericentric repeats (36). We observed that *Suv39h1* mRNA is increased initially in ac-

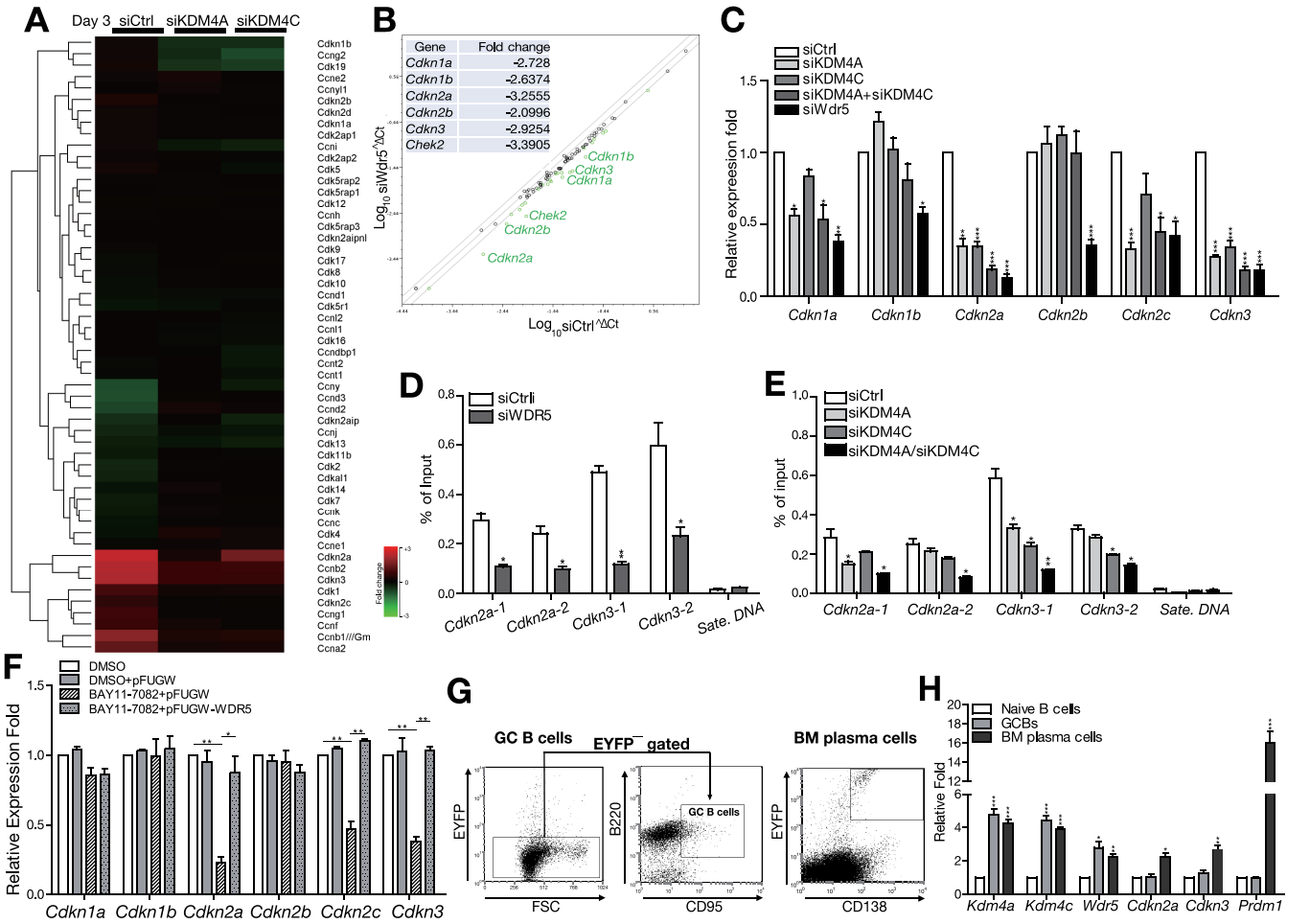

Figure 6. WDR5 controls the induction of CDKNs in the activation of B cells. (**A**) Heatmap showing the expression levels of several cell cycle-related genes after 3 days culturing of stimulated MD4 splenic B cells transfected with siCtrl, siKDM4A or siKDM4C. (**B**) Scatter plot of the results of RT-multiplex qPCR from stimulated MD4 B cells treated with either siWDR5-pools or siCtrl for 72 h. The most significantly reduced fold changes in gene expression in siWdr5 cells are indicated in the inserted table. (**C**) RT-qPCR validating that the mRNA levels of several *Cdkns* were decreased at 72 h in stimulated MD4 B cells transfected with siWDR5-pools, siKDM4A-pools and/or siKDM4C-pools. (**D**, **E**) ChIP showing the levels of H3K4me3 on the indicated gene loci in stimulated mouse MD4 B cells transfected with indicated siRNAs for 24 h. Satellite DNA (Sate. DNA) was used as the negative control locus. (**F**) The mRNA levels of indicated *Cdkns* at 72 h after stimulation with [HEL + anti-CD40 + IL-21] and treatment with the indicated reagents, DMSO or Bay11-7082, and/or lentiviral vector alone (pFUGW) or vector expressing WDR5, in MD4 B cells. (**G**, **H**) The indicated mRNA levels in $B220^+$ splenic B cells isolated from naïve C57BL/6 mice, $EYFP^-B220^+CD95^+$ GC B cells isolated from the spleen of *Prdm1*$^{EYFP/+}$ mice 2 weeks after primary immunization, and $EYFP^+CD138^+$ plasma cells isolated from the bone marrow of *Prdm1*$^{EYFP/+}$ mice 1 week after secondary immunization. The cell sorting strategies used to isolate splenic $EYFP^-B220^+CD95^+$ GC B and $EYFP^+CD138^+$ plasma cells are shown in (G). Results in (C), (D), (E), (F) and (H) are the mean ± SEM ($n = 3$). *$P < 0.05$, **$P < 0.01$, *** $P < 0.005$ (Student's *t*-test).

tivated B cells, but its expression does not correlate well with the global reduction of H3K9me2/me3 24–48 h after stimulation (Supplementary Figure S1A and E). Instead, we observed changes in the expression of the KDM4 family, particularly KDM4A and KDM4C, in both activated mouse and human B cells. The roles of KDM4 in cancer and its potential application as a therapeutic target have previously been reported (37,38). Both KDM4A and KDM4C are known to be important in development, such as in mouse embryonic stem cells (9,39). KDM4C has been shown to slow adipogenesis by attenuating the activity of the nuclear receptor PPARγ (40). It has also been reported that KDM4C interacts with KDM1A to collaboratively regulate the expression of androgen receptor-dependent genes (41). Here, we found that both KDM4A and KDM4C are induced following B cells exposed to Tfh-cell mimicking signals. The mechanism contributing to the induction of KDM4A and KDM4C awaits further elucidation. We think that KDM4A and KDM4C induction is independent of NF-κB activity because treatment with a NF-κB inhibitor did not seem to alter their expression (Figure 3D). In addition to being transcriptionally regulated, KDM4A or KDM4C activity can be modulated by interacting partners. Inositol hexakisphosphate kinase 1 has been shown to interact with KDM4C and affect its association with chromatin (42). It has been shown that the PI3K pathway regulates KDM4A localization and subsequent activity (43). Therefore, it is also possible that the activities of KDM4A and KDM4C in the present setting may be affected by their interacting partners. To further understand

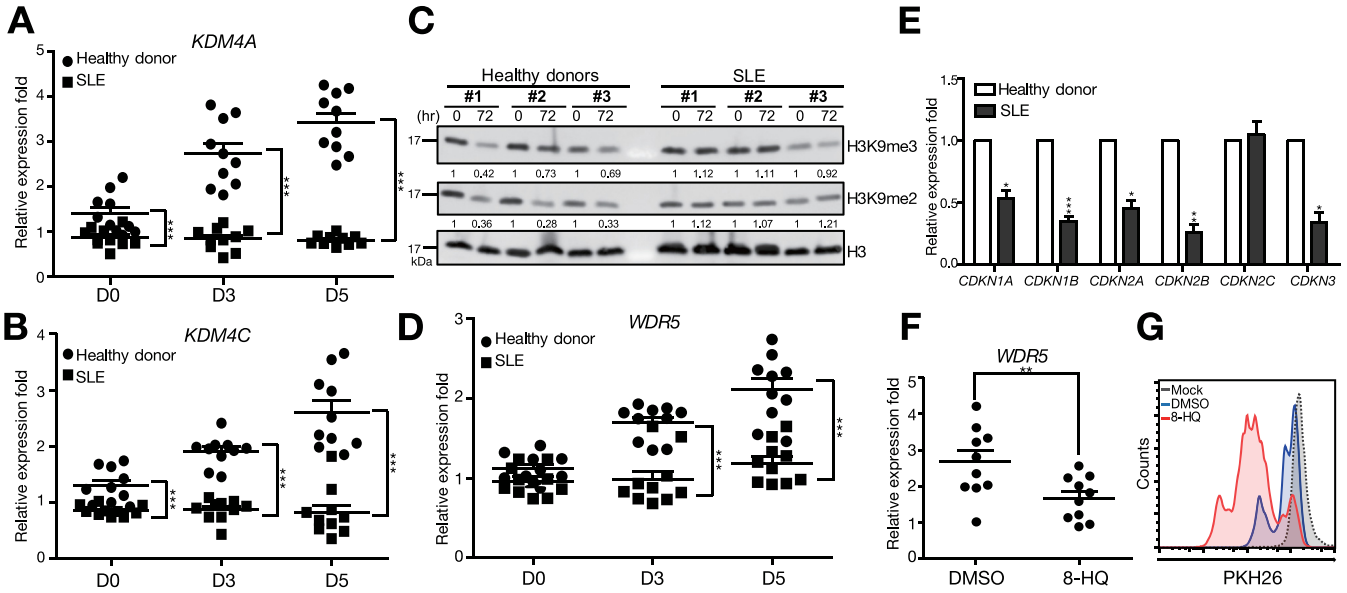

Figure 7. The expression of KDM4A, KDM4C and WDR5 is dys-regulated in SLE B cells. (A, B) mRNA levels of *KDM4A* (**A**) and *KDM4C* (**B**) in [anti-IgM + IL-21 + anti-CD40 + BAFF]-stimulated CD19$^+$ human B cells isolated from peripheral blood of healthy donors and SLE patients. (**C**) Immunoblotting showing the levels of H3K9me2/me3 histone marks at the indicated time point of [anti-IgM + IL-21 + anti-CD40 + BAFF]-stimulated CD19$^+$ human B cells isolated from three healthy donors and three SLE patients. (**D**) mRNA levels of *WDR5* in normal and SLE B cells as described in (A and B) at indicated days. (**E**) mRNA levels of various *CDKNs* in normal and SLE B cells as described in (A and B) at day 3. (**F**) *WDR5* mRNA levels in healthy donor peripheral blood B cells stimulated with anti-IgM + IL-21 + anti-CD40 + BAFF and treated with 8-HQ (200 μM) or DMSO for 3 days. (**G**) Analysis showing PKH26 dilution in stimulated healthy donor peripheral blood B cells treated with either 8-HQ or DMSO for 3 days. Results in (A), (B), (D), (E) and (F) represent the mean ± SEM ($n = 10$). *$P < 0.05$, **$P < 0.01$, ***$P < 0.005$ (Student's t-test).

the tissue-specificity of KDM4A/KDM4C targets, we analyzed the previously published ChIP-seq data of KDM4A and KDM4C targets in mouse acute myeloid leukemia cells (AML cells, accession number GSE81300) (24). Our combined bioinformatics analyses identified 335 genes significantly bound by KDM4A in AML cells, of which 28.4% overlapped with our KDM4A targets in B cells, and 359 genes significantly bound by KDM4C, of which 28% were commonly found in our KDM4C targets in B cells (Supplementary Figure S6A and Supplementary Table S2, sheets 2 and 3).

Among the various histone modifications that occur, H3K4me3 is considered to be a marker of actively transcribed genes (2,44). Methylation of H3K4 is mediated by methyltransferases such as WDR5-dependent COMPASS-family proteins (30). Here, we observed that *WDR5* is up-regulated by a KDM4A/KDM4C/NF-κB complex in stimulated B cells. Although global H3K4me3 levels are transiently increased 12 h after stimulation, this trend did not seem to be associated with the kinetics of WDR5 induction. We suspect that induction of WDR5 may not significantly alter global H3K4me3 levels in this context. Indeed, the correlation between H3K4me3 levels and the status of transcribed genes is ambiguous. High resolution ChIP-seq data show a significant enrichment of H3K4me3 between −200 bp and +50 bp of the activated genes, consistent with polymerase II binding profiles (2). It has also been reported that H3K4me3 islands are found to be associated with 59% of silent promoters (2).

To understand the whole picture of the regulatory complex of KDM4A and KDM4C, we applied ChIP-seq data of KDM4A and KDM4C binding profiles to compare the consensus binding of transcription factors. One transcription factor sharing a similar binding motif with KDM4A and KDM4C is NF-κB p65. Interestingly, our co-IP data show that KDM4A/KDM4C forms a complex with NF-κB at 24 h after stimulation but not at 48 h. We suspect that additional interacting partners or additional post-translational modifications may account for this temporal interaction. To comprehend the relationship between KDM4A/KDM4C and RELA, we compared the binding targets of NF-κB and KDM4A or KDM4C by using a published RELA ChIP-seq data from GEO database (accession number GSE36099) (22). Bioinformatics analyses revealed that 84 and 82 RELA binding genes were commonly found in our KDM4A and KDM4C ChIP-seq data, respectively. Particularly, RELA-bound genes were found in 34.1% of KDM4A and 31.0% of KDM4C targets, respectively, and *Wdr5* was one of them (Supplementary Figure S6A and Supplementary Table S4). However, while we show the binding of KDM4A/KDM4C to the NF-κB RELA subunit, we cannot exclude that other NF-κB subunits are involved because it has been demonstrated that RELA is dispensable for GC formation and affinity maturation *in vivo* (45).

Non-canonical NF-κB negatively regulates type 1 interferon by attenuating RELA/KDM4A complex binding at the *Ifnb* promoter after viral infection (46). However, the genome-wide targets of KDM4A and RELA in viral infection were not revealed. In another scenario, KDM4A cooperates with SRF/myocardin, the master transcription factor that controls cardiogenesis and differentiation of

smooth muscle cell lineages, to influence the expression of *Fhl1* through its H3K9me2/me3 specific demethylase activity (47). These studies show the importance of associations between KDM4 family members and vital transcription factors for gene expression regulation in physiological and infectious states. Our results reveal the importance of the temporal interaction of KDM4A/KDM4C/NF-κB in the control of induction of critical regulators in B cell activation and proliferation.

Alignments of various histone marks have shown that H3K9me2/me3 signals are higher in silent genes than active genes across a ±10 kb region surrounding the transcription start site (2). Our data show that KDM4A and KDM4C bind −12 kb upstream of *WDR5*. WDR5 has previously been shown to associate with the undifferentiated state of pluripotent stem cells (48), to be essential for vertebrate development (49), to be required for the recruitment of the transcription factor Myc to chromatin in tumorigenesis (50), and to play a role in cell cycle regulation in mixed-lineage leukemia (51). Inhibition of the activity of WDR5 by small molecules in mixed-lineage leukemia cells reduced cell proliferation and induced apoptosis (51). Prior to our present study, the regulation of WDR5 was largely unknown, and the targets of WDR5 and the detailed mode of action of WDR5 in B cell activation are still unknown. Nevertheless, we show for the first time in this study that WDR5 expression is controlled by a KDM4A/KDM4C/NF-κB complex and that several *Cdkns* are positively regulated by WDR5.

In this study, we found that, in response to Tfh cell-mimicking signals *in vitro*, the initiation of KDM4A/KDM4C/NF-κB epigenetic cascade may serve as the gatekeeper that regulates the cell cycle progression of activated B cells. Supporting this notion, our cDNA microarray data of the changes in gene expression in Tfh-signal primed B cells with KDM4A, KDM4C or WDR5 knockdown revealed that Cdkn2a and Cdkn3 may be involved. Cdkn3 has been reported to contribute to the maintenance of T cell homeostasis during infection (52), but its role in B cell activation has not been shown. CDKN2A (p16) is an important tumor suppressor gene that inhibits the assembly of CDKs by binding to CDK4 or CDK6, and CDKN2A mutations are associated with tumorigenesis (53). Of note, *Cdkn2a* is located in the susceptible locus of Balb/c mice for plasmacytoma (54). Cdkn2a expression also facilitates terminal differentiation of human adult brain tissue (55). These reports combined with our findings imply that KDM4A/KDM4C/NF-κB-mediated induction of Cdkn2 may have additional roles in favor of terminal differentiation of plasma cells, although it requires further experiments to demonstrate this hypothesis.

It is known that Tfh cells promote the expansion and differentiation of GC B cells. We here report a regulatory epigenetic pathway in activated B cells primed by Tfh cell-mimicking signals *in vitro* that guide the proper activation and proliferation of B cells. We demonstrated that, following stimulation, KDM4A and KDM4C are induced and temporally collaborate with NF-κB to regulate a panel of target genes. In particular, we found that WDR5 is a critical direct target of the KDM4A/KDM4C/NF-κB complex. Upon its activation, WDR5 then establishes the H3K4 methyltransferase complex at the promoter of several CDKNs, including *Cdkn2a* and *Cdkn3*, facilitating their expression and thereby modulating cell proliferation. Our results also suggest a new pathogenic alteration in SLE B cells that are inert in terms of the initiation of KDM4A/KDM4C epigenetic pathway after encountering Tfh signals. *KDM4A*, *KDM4C* and *WDR5*, as well as CDKNs are dysregulated in stimulated SLE B cells, supporting the hypothesis that some abnormal expression of histone modifiers is present in patients with SLE (56).

SUPPLEMENTARY DATA

Supplementary Data are available at NAR Online.

ACKNOWLEDGEMENTS

We thank the National Center for Genome Medicine of the National Core Facility Program for Biotechnology, Ministry of Science and Technology, Taiwan, for the bioinformatics support.

FUNDING

Academia Sinica [AS-105-TP-B08-1]; Ministry of Science and Technology, Taiwan [104-2320-B-001-016-MY3]. Funding for open access charge: Academia Sinica, Taiwan.
Conflict of interest statement. None declared.

REFERENCES

1. Kouzarides,T. (2007) Chromatin modifications and their function. *Cell*, **128**, 693–705.
2. Barski,A., Cuddapah,S., Cui,K., Roh,T.Y., Schones,D.E., Wang,Z., Wei,G., Chepelev,I. and Zhao,K. (2007) High-resolution profiling of histone methylations in the human genome. *Cell*, **129**, 823–837.
3. Kim,K.C., Geng,L. and Huang,S. (2003) Inactivation of a histone methyltransferase by mutations in human cancers. *Cancer Res.*, **63**, 7619–7623.
4. Mosammaparast,N. and Shi,Y. (2010) Reversal of histone methylation: biochemical and molecular mechanisms of histone demethylases. *Annu. Rev. Biochem.*, **79**, 155–179.
5. Shi,Y., Lan,F., Matson,C., Mulligan,P., Whetstine,J.R., Cole,P.A., Casero,R.A. and Shi,Y. (2004) Histone demethylation mediated by the nuclear amine oxidase homolog LSD1. *Cell*, **119**, 941–953.
6. Tsukada,Y., Fang,J., Erdjument-Bromage,H., Warren,M.E., Borchers,C.H., Tempst,P. and Zhang,Y. (2006) Histone demethylation by a family of JmjC domain-containing proteins. *Nature*, **439**, 811–816.
7. Pedersen,M.T. and Helin,K. (2010) Histone demethylases in development and disease. *Trends Cell Biol.*, **20**, 662–671.
8. Shi,Y. (2007) Histone lysine demethylases: emerging roles in development, physiology and disease. *Nat. Rev. Genet.*, **8**, 829–833.
9. Wu,L., Wary,K.K., Revskoy,S., Gao,X., Tsang,K., Komarova,Y.A., Rehman,J. and Malik,A.B. (2015) Histone demethylases KDM4A and KDM4C regulate differentiation of embryonic stem cells to endothelial cells. *Stem Cell Rep.*, **5**, 10–21.
10. Pedersen,M.T., Agger,K., Laugesen,A., Johansen,J.V., Cloos,P.A., Christensen,J. and Helin,K. (2014) The demethylase JMJD2C localizes to H3K4me3-positive transcription start sites and is dispensable for embryonic development. *Mol. Cell. Biol.*, **34**, 1031–1045.
11. Pedersen,M.T., Kooistra,S.M., Radzisheuskaya,A., Laugesen,A., Johansen,J.V., Hayward,D.G., Nilsson,J., Agger,K. and Helin,K. (2016) Continual removal of H3K9 promoter methylation by Jmjd2 demethylases is vital for ESC self-renewal and early development. *EMBO J.*, **35**, 1550–1564.

12. Harwood,N.E. and Batista,F.D. (2010) Early events in B cell activation. *Annu. Rev. Immunol.*, **28**, 185–210.
13. Nurieva,R.I., Chung,Y., Hwang,D., Yang,X.O., Kang,H.S., Ma,L., Wang,Y.H., Watowich,S.S., Jetten,A.M., Tian,Q. *et al.* (2008) Generation of T follicular helper cells is mediated by interleukin-21 but independent of T helper 1, 2, or 17 cell lineages. *Immunity*, **29**, 138–149.
14. Vinuesa,C.G., Tangye,S.G., Moser,B. and Mackay,C.R. (2005) Follicular B helper T cells in antibody responses and autoimmunity. *Nat. Rev. Immunol.*, **5**, 853–865.
15. Townsend,M.J., Monroe,J.G. and Chan,A.C. (2010) B-cell targeted therapies in human autoimmune diseases: an updated perspective. *Immunol. Rev.*, **237**, 264–283.
16. Chiu,Y.K., Lin,I.Y., Su,S.T., Wang,K.H., Yang,S.Y., Tsai,D.Y., Hsieh,Y.T. and Lin,K.I. (2014) Transcription factor ABF-1 suppresses plasma cell differentiation but facilitates memory B cell formation. *J. Immunol.*, **193**, 2207–2217.
17. Qin,X.F., An,D.S., Chen,I.S. and Baltimore,D. (2003) Inhibiting HIV-1 infection in human T cells by lentiviral-mediated delivery of small interfering RNA against CCR5. *Proc. Natl. Acad. Sci. U.S.A.*, **100**, 183–188.
18. Su,S.T., Ying,H.Y., Chiu,Y.K., Lin,F.R., Chen,M.Y. and Lin,K.I. (2009) Involvement of histone demethylase LSD1 in Blimp-1-mediated gene repression during plasma cell differentiation. *Mol. Cell. Biol.*, **29**, 1421–1431.
19. Langmead,B., Trapnell,C., Pop,M. and Salzberg,S.L. (2009) Ultrafast and memory-efficient alignment of short DNA sequences to the human genome. *Genome Biol.*, **10**, R25.
20. Zhang,Y., Liu,T., Meyer,C.A., Eeckhoute,J., Johnson,D.S., Bernstein,B.E., Nusbaum,C., Myers,R.M., Brown,M., Li,W. *et al.* (2008) Model-based analysis of ChIP-Seq (MACS). *Genome Biol.*, **9**, R137.
21. Salmon-Divon,M., Dvinge,H., Tammoja,K. and Bertone,P. (2010) PeakAnalyzer: genome-wide annotation of chromatin binding and modification loci. *BMC Bioinformatics*, **11**, 415.
22. Kieffer-Kwon,K.R., Nimura,K., Rao,S.S.P., Xu,J., Jung,S., Pekowska,A., Dose,M., Stevens,E., Mathe,E., Dong,P. *et al.* (2017) Myc regulates chromatin decompaction and nuclear architecture during B cell activation. *Mol. Cell*, **67**, 566–578.
23. Garber,M., Yosef,N., Goren,A., Raychowdhury,R., Thielke,A., Guttman,M., Robinson,J., Minie,B., Chevrier,N., Itzhaki,Z. *et al.* (2012) A high-throughput chromatin immunoprecipitation approach reveals principles of dynamic gene regulation in mammals. *Mol. Cell*, **47**, 810–822.
24. Agger,K., Miyagi,S., Pedersen,M.T., Kooistra,S.M., Johansen,J.V. and Helin,K. (2016) Jmjd2/Kdm4 demethylases are required for expression of Il3ra and survival of acute myeloid leukemia cells. *Genes Dev.*, **30**, 1278–1288.
25. Heinz,S., Benner,C., Spann,N., Bertolino,E., Lin,Y.C., Laslo,P., Cheng,J.X., Murre,C., Singh,H. and Glass,C.K. (2010) Simple combinations of lineage-determining transcription factors prime cis-regulatory elements required for macrophage and B cell identities. *Mol. Cell*, **38**, 576–589.
26. Maere,S., Heymans,K. and Kuiper,M. (2005) BiNGO: a Cytoscape plugin to assess overrepresentation of gene ontology categories in biological networks. *Bioinformatics*, **21**, 3448–3449.
27. Goodnow,C.C., Crosbie,J., Adelstein,S., Lavoie,T.B., Smith-Gill,S.J., Brink,R.A., Pritchard-Briscoe,H., Wotherspoon,J.S., Loblay,R.H., Raphael,K. *et al.* (1988) Altered immunoglobulin expression and functional silencing of self-reactive B lymphocytes in transgenic mice. *Nature*, **334**, 676–682.
28. Kim,J.Y., Kim,K.B., Eom,G.H., Choe,N., Kee,H.J., Son,H.J., Oh,S.T., Kim,D.W., Pak,J.H., Baek,H.J. *et al.* (2012) KDM3B is the H3K9 demethylase involved in transcriptional activation of lmo2 in leukemia. *Mol. Cell. Biol.*, **32**, 2917–2933.
29. Chen,Y.Q., Ghosh,S. and Ghosh,G. (1998) A novel DNA recognition mode by the NF-kappa B p65 homodimer. *Nat. Struct. Biol.*, **5**, 67–73.
30. Trievel,R.C. and Shilatifard,A. (2009) WDR5, a complexed protein. *Nat. Struct. Mol. Biol.*, **16**, 678–680.
31. Jorda,R., Paruch,K. and Krystof,V. (2012) Cyclin-dependent kinase inhibitors inspired by roscovitine: purine bioisosteres. *Curr. Pharm. Des.*, **18**, 2974–2980.
32. Kallies,A., Hasbold,J., Tarlinton,D.M., Dietrich,W., Corcoran,L.M., Hodgkin,P.D. and Nutt,S.L. (2004) Plasma cell ontogeny defined by quantitative changes in blimp-1 expression. *J. Exp. Med.*, **200**, 967–977.
33. King,O.N., Li,X.S., Sakurai,M., Kawamura,A., Rose,N.R., Ng,S.S., Quinn,A.M., Rai,G., Mott,B.T., Beswick,P. *et al.* (2010) Quantitative high-throughput screening identifies 8-hydroxyquinolines as cell-active histone demethylase inhibitors. *PLoS One*, **5**, e15535.
34. Baxter,J., Sauer,S., Peters,A., John,R., Williams,R., Caparros,M.L., Arney,K., Otte,A., Jenuwein,T., Merkenschlager,M. *et al.* (2004) Histone hypomethylation is an indicator of epigenetic plasticity in quiescent lymphocytes. *EMBO J.*, **23**, 4462–4472.
35. Whetstine,J.R., Nottke,A., Lan,F., Huarte,M., Smolikov,S., Chen,Z., Spooner,E., Li,E., Zhang,G., Colaiacovo,M. *et al.* (2006) Reversal of histone lysine trimethylation by the JMJD2 family of histone demethylases. *Cell*, **125**, 467–481.
36. Peters,A.H., O'Carroll,D., Scherthan,H., Mechtler,K., Sauer,S., Schofer,C., Weipoltshammer,K., Pagani,M., Lachner,M., Kohlmaier,A. *et al.* (2001) Loss of the Suv39h histone methyltransferases impairs mammalian heterochromatin and genome stability. *Cell*, **107**, 323–337.
37. Guerra-Calderas,L., Gonzalez-Barrios,R., Herrera,L.A., Cantu de Leon,D. and Soto-Reyes,E. (2015) The role of the histone demethylase KDM4A in cancer. *Cancer Genet.*, **208**, 215–224.
38. Berry,W.L. and Janknecht,R. (2013) KDM4/JMJD2 histone demethylases: epigenetic regulators in cancer cells. *Cancer Res.*, **73**, 2936–2942.
39. Sankar,A., Kooistra,S.M., Gonzalez,J.M., Ohlsson,C., Poutanen,M. and Helin,K. (2017) Maternal expression of the histone demethylase Kdm4a is crucial for pre-implantation development. *Development*, **144**, 3264–3277.
40. Lizcano,F., Romero,C. and Vargas,D. (2011) Regulation of adipogenesis by nuclear receptor PPARgamma is modulated by the histone demethylase JMJD2C. *Genet. Mol. Biol.*, **34**, 19–24.
41. Wissmann,M., Yin,N., Muller,J.M., Greschik,H., Fodor,B.D., Jenuwein,T., Vogler,C., Schneider,R., Gunther,T., Buettner,R. *et al.* (2007) Cooperative demethylation by JMJD2C and LSD1 promotes androgen receptor-dependent gene expression. *Nat. Cell Biol.*, **9**, 347–353.
42. Burton,A., Azevedo,C., Andreassi,C., Riccio,A. and Saiardi,A. (2013) Inositol pyrophosphates regulate JMJD2C-dependent histone demethylation. *Proc. Natl. Acad. Sci. U.S.A.*, **110**, 18970–18975.
43. Salifou,K., Ray,S., Verrier,L., Aguirrebengoa,M., Trouche,D., Panov,K.I. and Vandromme,M. (2016) The histone demethylase JMJD2A/KDM4A links ribosomal RNA transcription to nutrients and growth factors availability. *Nat. Commun.*, **7**, 10174.
44. Henikoff,S. and Shilatifard,A. (2011) Histone modification: cause or cog? *Trends Genet.*, **27**, 389–396.
45. Heise,N., De Silva,N.S., Silva,K., Carette,A., Simonetti,G., Pasparakis,M. and Klein,U. (2014) Germinal center B cell maintenance and differentiation are controlled by distinct NF-kappaB transcription factor subunits. *J. Exp. Med.*, **211**, 2103–2118.
46. Jin,J., Hu,H., Li,H.S., Yu,J., Xiao,Y., Brittain,G.C., Zou,Q., Cheng,X., Mallette,F.A., Watowich,S.S. *et al.* (2014) Noncanonical NF-kappaB pathway controls the production of type I interferons in antiviral innate immunity. *Immunity*, **40**, 342–354.
47. Zhang,Q.J., Chen,H.Z., Wang,L., Liu,D.P., Hill,J.A. and Liu,Z.P. (2011) The histone trimethyllysine demethylase JMJD2A promotes cardiac hypertrophy in response to hypertrophic stimuli in mice. *J. Clin. Invest.*, **121**, 2447–2456.
48. Ang,Y.S., Tsai,S.Y., Lee,D.F., Monk,J., Su,J., Ratnakumar,K., Ding,J., Ge,Y., Darr,H., Chang,B. *et al.* (2011) Wdr5 mediates self-renewal and reprogramming via the embryonic stem cell core transcriptional network. *Cell*, **145**, 183–197.
49. Wysocka,J., Swigut,T., Milne,T.A., Dou,Y., Zhang,X., Burlingame,A.L., Roeder,R.G., Brivanlou,A.H. and Allis,C.D. (2005) WDR5 associates with histone H3 methylated at K4 and is essential for H3 K4 methylation and vertebrate development. *Cell*, **121**, 859–872.
50. Thomas,L.R., Wang,Q., Grieb,B.C., Phan,J., Foshage,A.M., Sun,Q., Olejniczak,E.T., Clark,T., Dey,S., Lorey,S. *et al.* (2015) Interaction with WDR5 promotes target gene recognition and tumorigenesis by MYC. *Mol. Cell*, **58**, 440–452.

51. Cao,F., Townsend,E.C., Karatas,H., Xu,J., Li,L., Lee,S., Liu,L., Chen,Y., Ouillette,P., Zhu,J. *et al.* (2014) Targeting MLL1 H3K4 methyltransferase activity in mixed-lineage leukemia. *Mol. Cell*, **53**, 247–261.
52. Chen,C.F., Feng,X., Liao,H.Y., Jin,W.J., Zhang,J., Wang,Y., Gong,L.L., Liu,J.J., Yuan,X.H., Zhao,B.B. *et al.* (2014) Regulation of T cell proliferation by JMJD6 and PDGF-BB during chronic hepatitis B infection. *Sci. Rep.*, **4**, 6359.
53. Sherr,C.J. and Roberts,J.M. (1995) Inhibitors of mammalian G1 cyclin-dependent kinases. *Genes Dev.*, **9**, 1149–1163.
54. Zhang,S., Ramsay,E.S. and Mock,B.A. (1998) Cdkn2a, the cyclin-dependent kinase inhibitor encoding p16INK4a and p19ARF, is a candidate for the plasmacytoma susceptibility locus, Pctr1. *Proc. Natl. Acad. Sci. U.S.A.*, **95**, 2429–2434.
55. Lois,A.F., Cooper,L.T., Geng,Y., Nobori,T. and Carson,D. (1995) Expression of the p16 and p15 cyclin-dependent kinase inhibitors in lymphocyte activation and neuronal differentiation. *Cancer Res.*, **55**, 4010–4013.
56. Gray,S.G. (2013) Perspectives on epigenetic-based immune intervention for rheumatic diseases. *Arthritis Res. Ther.*, **15**, 207.